A Dual-Band Terahertz Leaky-Wave Meta-Antenna

Yitao Ouyang, Yuanzhi Liu, Min Zhang, Hong Su, Yejun He, *Senior Member, IEEE,* and Huawei Liang

***Abstract*—A leaky-wave meta-antenna (LWMA) is first proposed for high-gain co-aperture control of dual-band terahertz (THz) waves, where the meta-slots enable independent full-phase manipulation of two orthogonal waves at distinct frequencies. When used as a transmitting antenna, *x*- and *y*-polarized guided waves at the frequencies of 0.14 THz and 0.0972 THz, respectively, are coupled into the parallel-plate metal waveguide via two separate waveguide input ports. The two guided waves are manipulated simultaneously and independently by the meta-slots, enabling directional radiation through a shared aperture. The far-field gains are 35.1 dBi at 0.14 THz and 32 dBi at 0.0972 THz, with aperture efficiencies of 43.8% and 44.6%, respectively. The corresponding cross-polarization levels are –42.8 dB and –31.2 dB below the main lobes, and the isolation levels are as low as –31.3 dB and –31.1 dB. When operated in reverse as a receiving antenna, it converts the two orthogonally polarized incident beams into two-dimensional guided waves, which are then focused onto two distinct receiving ports. The gains at the focal points are 27 dB at 0.14 THz and 26.3 dB at 0.0972 THz. Both the measured far-field radiation patterns and intensity distributions on the focal planes agree well with the simulation results. The dual-band THz LWMA is promising for applications in sixth-generation mobile communications, radar detection, and imaging.**

***Index Terms*—leaky-wave meta-antenna (LWMA), terahertz (THz), dual-band, full phase manipulation, high gain**

I. Introduction

THE dramatic rise in communication data volume has led to an unprecedented spectrum scarcity in conventional frequency bands for mobile communication systems [1]. The terahertz (THz) band, ranging from 0.1 THz to 10 THz, emerges as a pivotal solution to address the escalating demand for high-capacity wireless communication, owing to its ultra-broad bandwidth [2–6]. However, the severe free-space path loss of THz waves fundamentally limits their effective propagation range. Thus, it is a critical requirement to design and fabricate high-gain THz antennas for advancing sixth-generation wireless communication systems [7–11].

Leaky-wave antennas (LWAs) are widely used in wireless communications owing to their intrinsic advantages of high directivity, low-profile form factor, and structurally simple configuration [12–15]. In LWAs, guided waves propagate along a waveguide or transmission line and gradually leak into free space through periodic discontinuities or slots. The radiation direction, phase, and amplitude of the emitted beam are controlled by the unit structure, spacing, and the propagation constant of the guided wave, enabling beam steering and high-gain radiation [16–19]. Various LWAs have been proposed based on different radiation mechanisms, including uniform, quasi-uniform, and periodic LWAs [20–23]. Oliner proposed a simple LWA composed of a length of uniform microstrip line excited in its first higher-order mode, which becomes leaky near the cutoff frequency, enabling efficient radiation with most of the leakage occurring as space waves [24]. A compact dual-polarized Fabry–Perot quasi-uniform LWA was presented for full-duplex broadband applications, offering high gain, high isolation, and dual-linear polarization [25]. Zhao et al. proposed a two-dimensional (2D) periodic LWA with a slot array on a grounded dielectric slab, featuring high directivity and good broadside circular polarization [26].

In the THz regime, LWAs have also attracted great attention. Karl et al. demonstrated frequency-division multiplexing and demultiplexing using a THz LWA based on a metal parallel-plate waveguide, achieving operation over more than one octave of bandwidth [27]. Guerboukha et al. reported a THz LWA with trapezoidal slot structures, achieving a gain of 24.3 dB at 200 GHz [28]. Hongjian et al. developed an LWA based on a groove gap waveguide, achieving a gain exceeding 15 dB over the operational frequency band from 430 to 560 GHz [29]. Lu et al. demonstrated an InP-based THz beam-steering LWA, with a scan angle ranging from –46° to +42° and an average gain of 11 dBi [30]. Although various functions have been realized by these THz LWAs, the lack of phase control capability has a negative impact on the antenna performance. In contrast, the integration of THz LWAs with metasurfaces enables precise beamforming through the tailored phase modulation of each unit cell, which can further expand their application potential. Peng et al. proposed a THz leaky-wave meta-antenna (LWMA) with a rectangular slot array, where each slot enables distinct phase control for the outgoing beam via tailored dimensions [31]. Similar to the aforementioned LWAs, this LWMA is still limited to single-band operation, although dual-band antennas are capable of enhancing channel capacity and meeting multi-band operational requirements [32–35]. Currently, the realization of dual-band LWMAs remains quite challenging in the THz regime.

In this study, a dual-band leaky-wave meta-antenna (DB-LWMA) is proposed for high-gain transmission and reception of THz waves. When employed as a transmitting antenna, x- and y-polarized waves with frequencies of 0.14 THz and 0.0972 THz are fed via two rectangular waveguide ports,

Manuscript received July 16, 2025. This work was supported in part by the National Key Research and Development Program of China under Grant 2023YFE0107900, the Guangdong Basic and Applied Basic Research Foundation, China under Grant No. 2025A1515011508, and the Shenzhen Basic Research Special Project under Grant No. JCYJ20240813141606009. (Corresponding Authors: Huawei Liang, Yejun He)

Yitao Ouyang, Yuanzhi Liu, Min Zhang, Hong Su and Huawei Liang are with Key Laboratory of Optoelectronic Devices and Systems of Ministry of Education and Guangdong Province, Shenzhen University, Shenzhen 518060, P. R. China (e-mail: 2310452038@email.szu.edu.cn; 2210452068@szu.edu.cn; zhangmin@szu.edu.cn; hsu@szu.edu.cn; hwliang@szu.edu.cn).

Yejun He and Huawei Liang are with State Key Laboratory of Radio Frequency Heterogeneous Integration, Shenzhen University, Shenzhen 518060, P. R. China (e-mail: heyejun@126.com).

This article has been accepted for publication in Journal of Lightwave Technology. This is the author's version which has not been fully edited and content may change prior to final publication. Citation information: DOI 10.1109/JLT.2025.3620946

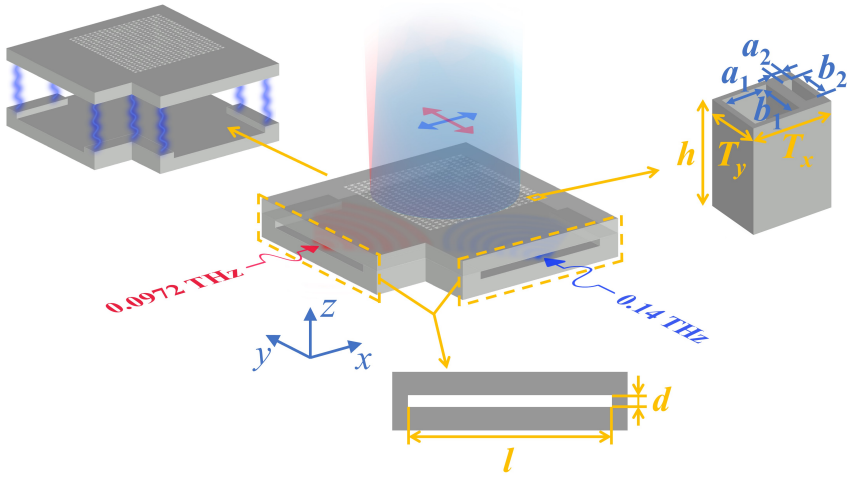

Fig. 1. Structural configuration of DB-LWMA for high-gain co-aperture transmission control of dual-band THz waves.

respectively, and propagate in the parallel-plate metal waveguide (PPMW). Different from slots in conventional LWAs [26, 28], simultaneous and independent full-phase control of dual guided modes can be achieved via precisely engineered aperture dimensions in the slotted meta-units. The antenna with a radiating aperture of 53 mm × 53 mm achieves gains of 35.1 dBi at 0.14 THz and 32 dBi at 0.0972 THz, with aperture efficiencies (AEs) of 43.8% and 44.6%, respectively. The corresponding cross-polarization levels are –42.8 dB and –31.2 dB below the main lobes, and the isolation levels are as low as –31.3 dB and –31.1 dB. When operated in reverse as a receiving antenna, orthogonally polarized incident waves are converted into guided waves by the meta-slot array. They can be focused onto two different receiving ports due to the phase control of the meta-slots. The beam-focusing gains are 27 dB at 0.14 THz and 26.3 dB at 0.0972 THz, respectively, and the corresponding efficiencies are 48.9% and 50.8%. Based on the design, an antenna prototype was fabricated and experimentally measured, with the results exhibiting good agreement with the simulation data.

II. Antenna Design and Analysis

Fig. 1 illustrates the structural configuration of the DB-LWMA, comprising two PPMWs and an array of meta-slots engraved on one side of their overlapping region. The operating frequencies of the antenna are selected as 0.14 THz and 0.0972 THz, which exhibit relatively low atmospheric absorption and hold great application potential in sixth-generation mobile communications [36, 37]. x- and y-polarized waves with frequencies of 0.14 THz and 0.0972 THz, fed via two different waveguide ports, can propagate as 2D cylindrical guided modes within the PPMW structures with a thickness of d = 3 mm and a width of l = 53 mm [31].

The PPMW, comprising two parallel metallic plates, can guide THz waves with low propagation loss. Boundary reflections perpendicular to the input ports are negligible because the transverse dimensions are much larger than the operational wavelengths. The phase variation characteristics of transverse electric (TE) modes in the waveguide can be determined by the propagation constant β, expressed as:

$$\beta = \sqrt{k^2 - (\frac{m\pi}{d})^2} \tag{1}$$

where $k = 2\pi/\lambda$ is the wave vector, λ is the operating wavelength, m is the order of the TE guided mode, and d is the plate separation. The rectangular meta-slots with a depth h = 6 mm enable energy leakage into free space, and the phase delay of two orthogonally polarized waves can be controlled independently at the same time by the meta-slot array with a dimension of 53 mm × 53 mm.

The AE is an important parameter of an LWA, defined as the ratio of the antenna's effective aperture area to its physical aperture area. In LWAs, the active radiating spacing along the propagation direction strongly influences the attenuation constant. Insufficient spacing results in an increased leakage rate, whereby the guided energy is radiated too rapidly, leading to a substantial degradation of AE. Hence, appropriate selection of the radiating spacing along the propagation direction is crucial for achieving high-performance leaky-wave antennas [38, 39]. Full-wave electromagnetic simulations are performed to calculate the AEs of the dual-band LWA at both operating frequencies using the commercial software COMSOL Multiphysics. Aluminum is selected as the metallic material, and its relative permittivity is described by the Drude model [40]. The relative permittivity of air inside the PPMW and meta-slots is 1. The air layer outside the radiating surface is used to simulate guided waves leaking into free space through the array of meta-slots, with scattering boundary conditions applied to the outer surface. x-polarized waves at 0.14 THz and y-polarized waves at 0.0972 THz are independently excited through separate input ports and propagate as one-dimensional (1D) guided TE modes, as shown in Figs. 2(a) and 2(c), respectively. By the control of the meta-slots, the two guided modes gradually radiate into free space, as shown in Figs. 2(b)

This article has been accepted for publication in Journal of Lightwave Technology. This is the author's version which has not been fully edited and content may change prior to final publication. Citation information: DOI 10.1109/JLT.2025.3620946

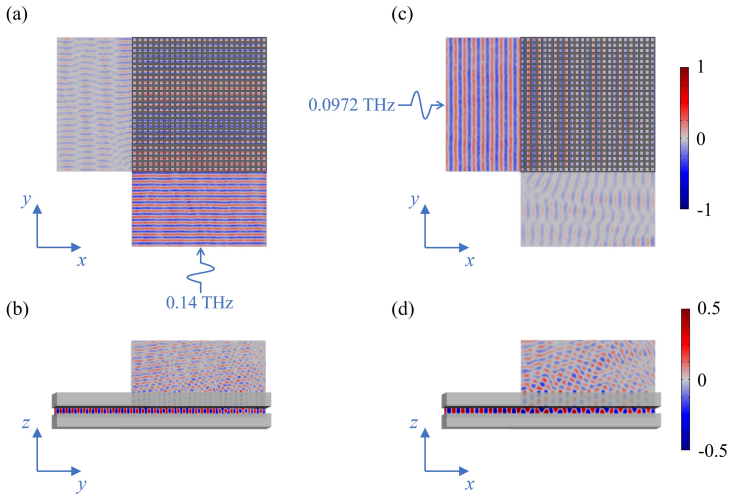

Fig. 2. Orthogonally polarized waves with frequencies of 0.14 THz and 0.0972 THz, coming from separate input ports respectively, propagate in PPMW as 1D guided modes and gradually radiate into free space. Electric field distributions of x-polarized waves in (a) x-y and (b) y-z planes. Electric field distributions of y-polarized waves in (c) x-y and (d) x-z planes.

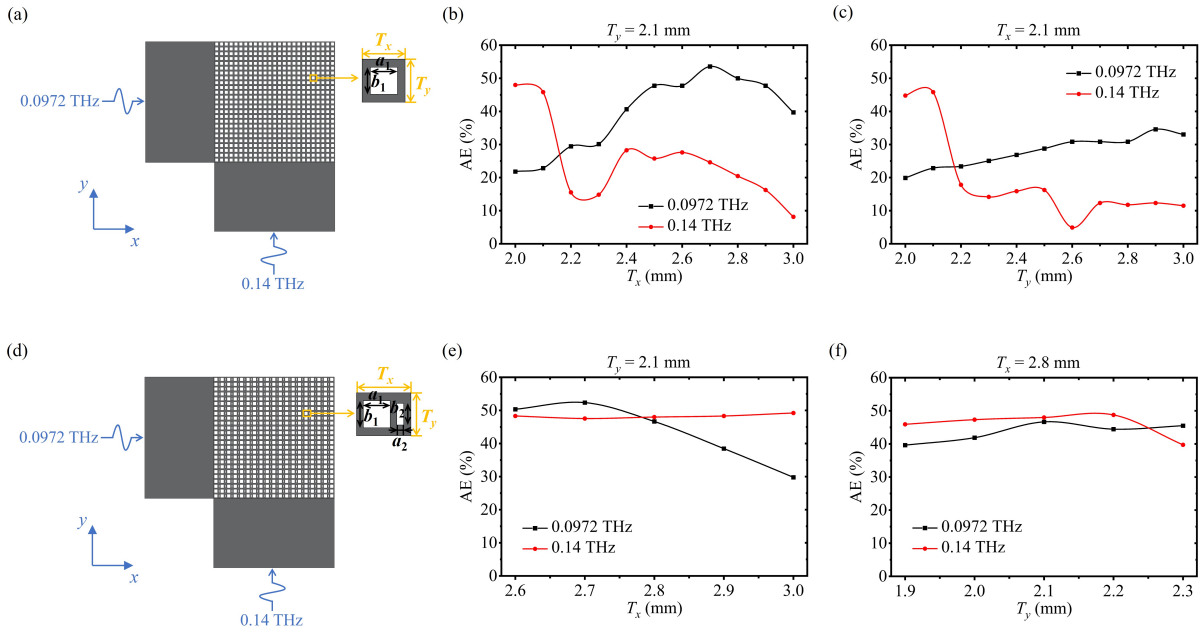

Fig. 3. (a) Schematic of LWMA with a single slot in each unit cell. Dependences of AEs on (b) T_x and (c) T_y for LWMA with single-slot unit cells. (d) Schematic of LWMA with dual slots in each unit cell. Dependences of AEs on (e) T_x and (f) T_y for LWMA with dual-slot unit cells.

and 2(d). According to the waveguide theory, the rectangular aperture dimension perpendicular to the polarization direction should be larger than $\lambda/2$ to avoid the mode cutoff [41]. As illustrated in Fig. 3(a), the array for simultaneously controlling x- and y-polarized waves contains one slot in each unit cell, where the side lengths along y- and x-axes are larger than half-wavelengths of the x-polarized wave and the y-polarized wave, respectively. The antenna aperture is 53 mm × 53 mm, with a thickness of the PPMW d = 3 mm. When the side lengths of the rectangular meta-slots are all 1.67 mm along x-axis and 1.42 mm along y-axis, the dependences of AEs on the x- and y-directional dimensions of the unit cell (T_x and T_y) are calculated. As shown in Figs. 3(b) and 3(c), the AEs at the frequencies of 0.14 THz and 0.0972 THz cannot simultaneously exceed 30% when the structure varies in the adopted range. Thus, obtaining high AEs at both frequencies is quite challenging by using the unit cell with only a single slot inside due to the significant wavelength difference between the two waves.

To overcome the limit of the single-slot unit cells, the structure with dual slots in each unit cell is introduced, as shown in Fig. 3(d). Both x- and y-polarized guided waves can

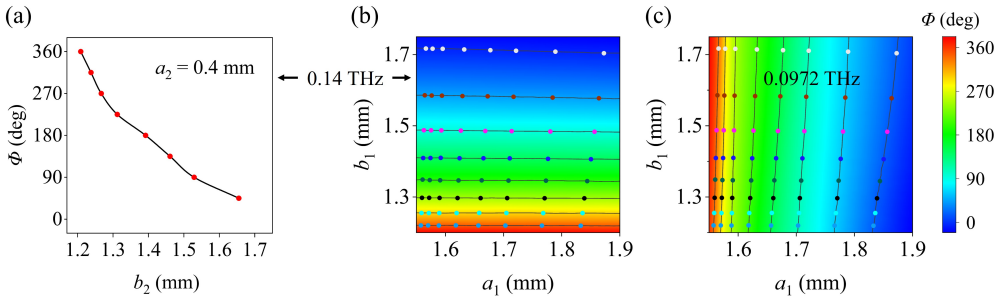

Fig. 4. (a) Dependences of phase delay at frequency of 0.14 THz on b_2 for the smaller meta-slots. Phase delays at frequencies of (b) 0.14 THz and (c) 0.0972 THz as functions of side lengths a_1 and b_1.

TABLE I
DIMENSIONS (b_2) OF THE SMALLER META-SLOTS WITH a_2 = 0.4 MM

Value (mm)							
1.209	1.238	1.267	1.312	1.392	1.461	1.529	1.655

TABLE II
DIMENSIONS (a_1, b_1) OF THE LARGER META-SLOTS

Value (mm)							
(1.569,1.732)	(1.58,1.73)	(1.599,1.729)	(1.64,1.727)	(1.678,1.725)	(1.722,1.72)	(1.79,1.713)	(1.874,1.705)
(1.567,1.597)	(1.578,1.597)	(1.598,1.596)	(1.636,1.594)	(1.674,1.593)	(1.718,1.591)	(1.785,1.588)	(1.865,1.582)
(1.565,1.492)	(1.577,1.492)	(1.597,1.491)	(1.633,1.491)	(1.669,1.49)	(1.714,1.49)	(1.78,1.489)	(1.859,1.488)
(1.564,1.407)	(1.576,1.407)	(1.596,1.408)	(1.63,1.408)	(1.666,1.408)	(1.711,1.408)	(1.777,1.409)	(1.853,1.409)
(1.561,1.343)	(1.575,1.343)	(1.594,1.343)	(1.627,1.343)	(1.663,1.343)	(1.709,1.344)	(1.774,1.344)	(1.847,1.344)
(1.561,1.293)	(1.574,1.294)	(1.593,1.294)	(1.625,1.294)	(1.659,1.294)	(1.707,1.294)	(1.771,1.294)	(1.841,1.294)
(1.561,1.253)	(1.573,1.253)	(1.593,1.253)	(1.624,1.253)	(1.658,1.252)	(1.705,1.252)	(1.768,1.252)	(1.837,1.252)
(1.56,1.22)	(1.572,1.22)	(1.592,1.219)	(1.622,1.219)	(1.656,1.219)	(1.703,1.218)	(1.766,1.218)	(1.833,1.217)

leak into free space through the larger meta-slots. However, only x-polarized guided waves can pass through the smaller meta-slots with a side length along the x-axis of $a_2 = 0.4$ mm, as this dimension is much smaller than the half-wavelength of the y-polarized waves. The center-to-center distance of the two slots in a unit cell is set to $T_x/2$, where T_x is the x-directional dimension of the unit cell. Consequently, in the x-direction, the active radiating spacings are T_x and $T_x/2$ for the y- and x-polarized waves, respectively, while the y-directional active radiating spacings are T_y for both waves, which enables comparable AEs for the two waves with significant wavelength difference. The AEs of the LWMA with dual slots in each unit cell are calculated. As illustrated in Figs. 3(e) and 3(f), when $T_x = 2.8$ mm and $T_y = 2.1$ mm, the AEs of the two orthogonally polarized waves are both higher than 45%. The antenna aperture remains 53 mm × 53 mm and the thickness of the PPMW is still 3 mm. The dimensions of the two meta-slots are 1.67 mm × 1.42 mm and 0.4 mm × 1.42 mm, respectively.

The phase delay of the two orthogonally polarized waves passing through the meta-slots, ϕ, can be tuned by adjusting the slot dimensions, which are numerically analyzed using COMSOL Multiphysics software. A field probe is positioned at the geometric center of the output surface to record the phase of transmitted waves. For the smaller meta-slot with x-directional length $a_2 = 0.4$ mm, the phase delay at the frequency of 0.14 THz as a function of the side length along the y-axis, b_2, is shown in Fig. 4(a). Eight meta-slots are selected to cover the phase range of 0°–360° with an interval of 45°, whose dimensions are listed in Table I. For the larger meta-slots, the dependences of the phase delay at the frequencies of 0.14 THz (x-polarized) and 0.0972 THz (y-polarized) on the side lengths (a_1 and b_1) were calculated, as shown in Figs. 4(b) and 4(c), respectively. The 64 intersection points of these contours correspond to selected meta-slots, which can cover the phase range of 0°–360° with an interval of 45° for both frequencies. The corresponding dimensions (a_1, b_1) are listed in Table II.

In the simulation, two rectangular waveguide ports with dimensions of 3 mm × 3 mm are used as feed sources for both x- and y-polarized waves. Due to the z-directional confinement, the two orthogonally polarized waves propagate freely in x-y plane with cylindrical wavefronts of finite height,

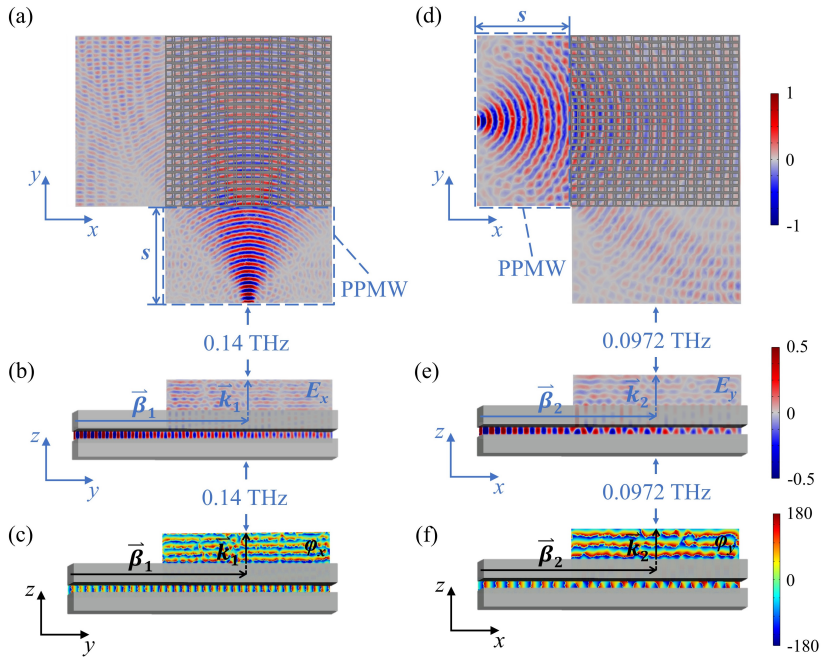

Fig. 5. DB-LWMA for independent control of two orthogonally polarized waves at frequencies of 0.14 THz and 0.0972 THz. Electric field distributions of x-polarized waves in (a) x-y and (b) y-z planes. Phase distribution of x-polarized waves in (c) y-z plane. Electric field distributions of y-polarized waves in (d) x-y and (e) x-z planes. Phase distribution of y-polarized waves in (f) x-z plane.

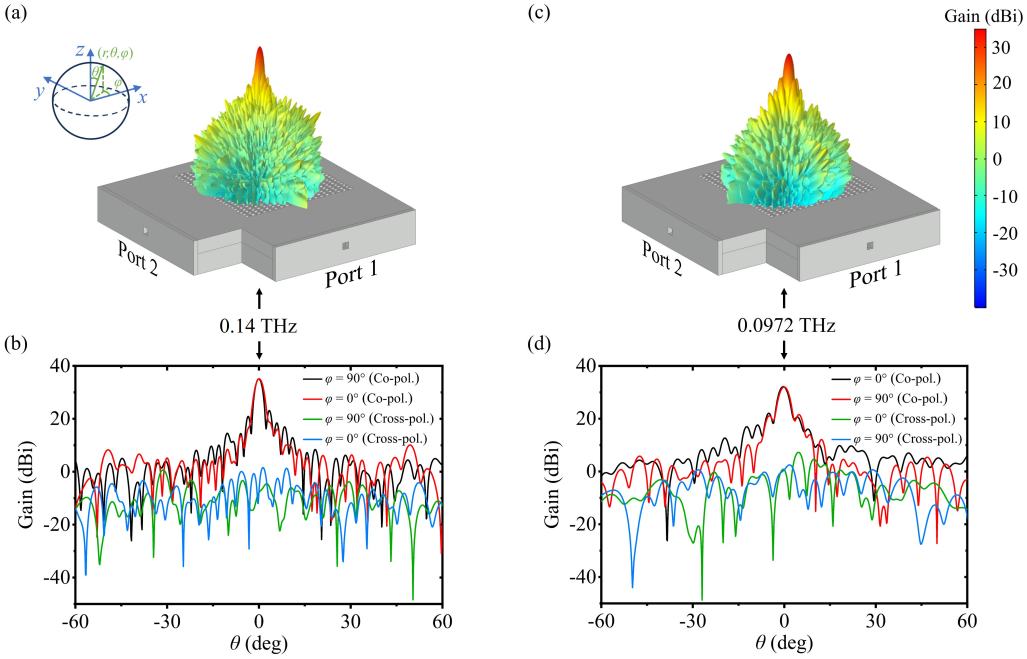

Fig. 6. Far-field radiation characteristics of DB-LWMA. (a) 3D radiation pattern and (b) radiation patterns in H- ($\varphi = 90°$) and E-planes ($\varphi = 0°$) of co- and cross-polarized waves at the frequency of 0.14 THz. (c) 3D radiation pattern and (d) radiation patterns in H- ($\varphi = 0°$) and E-planes ($\varphi = 90°$) of co- and cross-polarized waves at the frequency of 0.0972 THz.

as shown in Figs. 5(a) and 5(d). The distances between the ports and the meta-slots, s, are both 30 mm. The width of the PPMW l = 53 mm, is much larger than the wavelength. Thus, the minor wavefront distortion near the boundaries caused by the reflections is typically negligible. The propagation constant remains identical in different directions, so the phase distributions for the two waves can be given by:

$$\varphi_1(x, y) = \varphi_{01} + \beta_1 R_1(x, y) \tag{2}$$

$$\varphi_2(x, y) = \varphi_{02} + \beta_2 R_2(x, y) \tag{3}$$

where φ_{01} and φ_{02} are the initial phases of the x-polarized and y-polarized waves at the waveguide feed ports, respec-

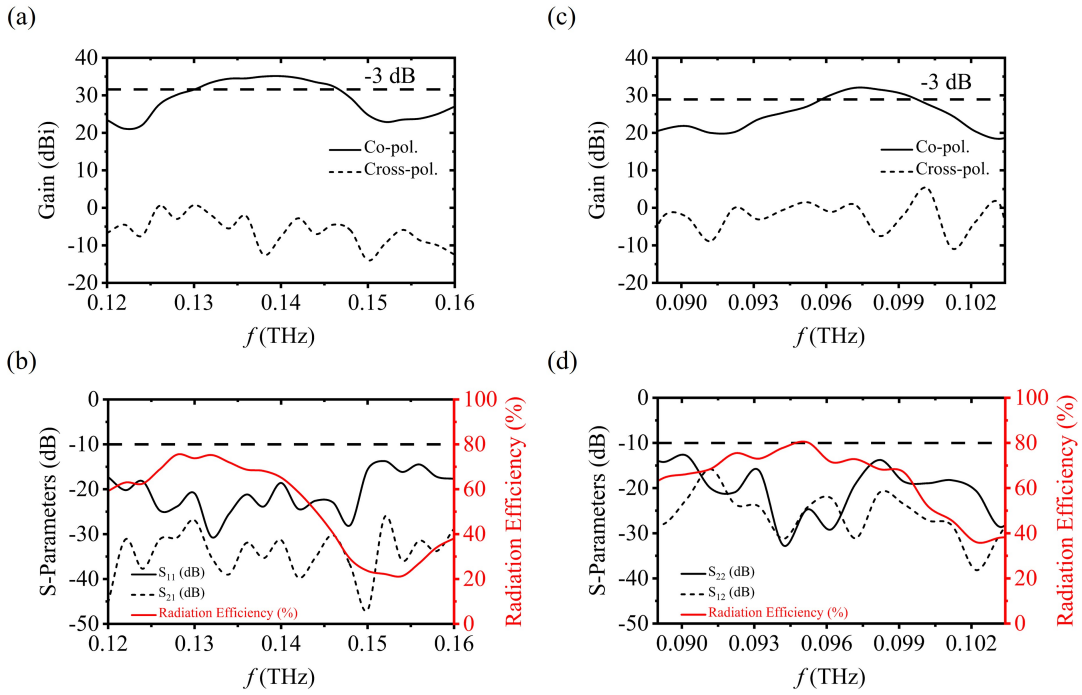

Fig. 7. Performance characteristics of DB-LWMA. (a) Co- and cross-polarization in the main-lobe direction; (b) reflection coefficients (S_{11}), isolation levels (S_{21}), and radiation efficiencies as functions of frequency for x-polarized waves. (c) Co- and cross-polarization in the main-lobe direction; (d) reflection coefficients (S_{22}), isolation levels (S_{12}), and radiation efficiencies as functions of frequency for y-polarized waves.

tively. $R_1(x, y)$ and $R_2(x, y)$ represent the distances from the corresponding ports to each meta-slot. β_1 and β_2 are the propagation constants of the first-order modes, which can be calculated by Eq. 1. According to Eqs. 2 and 3, the phases of the two waves arriving at each meta-slot can be calculated. To achieve high gain, the phase distribution on the output surface of the DB-LWMA should be uniform. This requirement can be fulfilled by judiciously arranging the rectangular meta-slots from Tables I and II, which serve as phase-controlling unit cells. Unlike the slots used in traditional LWAs [26, 28], the dimensions of these subwavelength rectangular slots are engineered to impart tailored phase delays, enabling precise phase compensation [42]. As a result, the two guided waves leak into free space as plane waves, as shown in Figs. 5(b) and 5(e), and their phase distributions are illustrated in Figs. 5(c) and 5(f). Furthermore, by tailoring the geometrical parameters of the meta-slots, the antenna can generate a variety of desired wavefronts, such as a directional beam at a specific angle or multiple beams. Compared to conventional LWAs, the DB-LWMA has the advantage of achieving high-gain co-aperture control of dual-band THz waves [43].

III. Simulation and Measurement Results

A. Transmission

The three-dimensional (3D) far-field radiation pattern of x-polarized waves at the frequency of 0.14 THz (Port 1 excitation) is shown in Fig. 6(a), and the corresponding 2D radiation patterns in H- and E-planes are shown in Fig. 6(b). The peak gain is as high as 35.1 dBi with an AE of 43.8%, and the 3-dB beamwidths in H- and E-planes are 2.2° and 2.5°, respectively, alongside sidelobe levels of 12 dB and 19.1 dB below the main lobe. The y-polarized waves at the frequency of 0.0972 THz (Port 2 excitation) share the same radiation aperture, and the 3D and 2D far-field radiation patterns are displayed in Figs. 6(c) and 6(d), respectively. The peak gain is 32 dBi with an AE of 44.6%, and the 3-dB beamwidths in H- and E-planes are 3.1° and 3.2°, respectively, alongside sidelobe levels of 10 dB and 10.5 dB below the main lobe. Thus, dual-band high-gain THz emission can be realized using the DB-LWMA even without complex feed networks. As shown in Figs. 7(a) and 7(c), the 3-dB gain bandwidths of x- and y-polarized waves span from 0.13 to 0.146 THz (16 GHz) and from 0.096 to 0.1 THz (4 GHz), respectively, with the cross-polarization levels of –42.8 dB and –31.2 dB below the main lobes. The reflection coefficients remain below -10 dB for the x-polarized waves in the frequency range of 0.12–0.16 THz and the y-polarized waves in the range of 0.089–0.1034 THz, as shown in Figs. 7(b) and 7(d). The isolation levels are as low as –31.3 dB at 0.14 THz and –31.1 dB at 0.0972 THz, demonstrating excellent decoupling performance for compact dual-polarized THz antennas [44]. Additionally, the radiation efficiencies reach 65.2% at 0.14 THz and 72.8% at 0.0972 THz, which can be further improved by increasing the radiation aperture area [45].

According to the design above, a DB-LWMA prototype was fabricated using wire electrical discharge machining (WEDM). The integrated prototype structure is displayed in Fig. 8(a), and a top view of its two separated components and two adapter

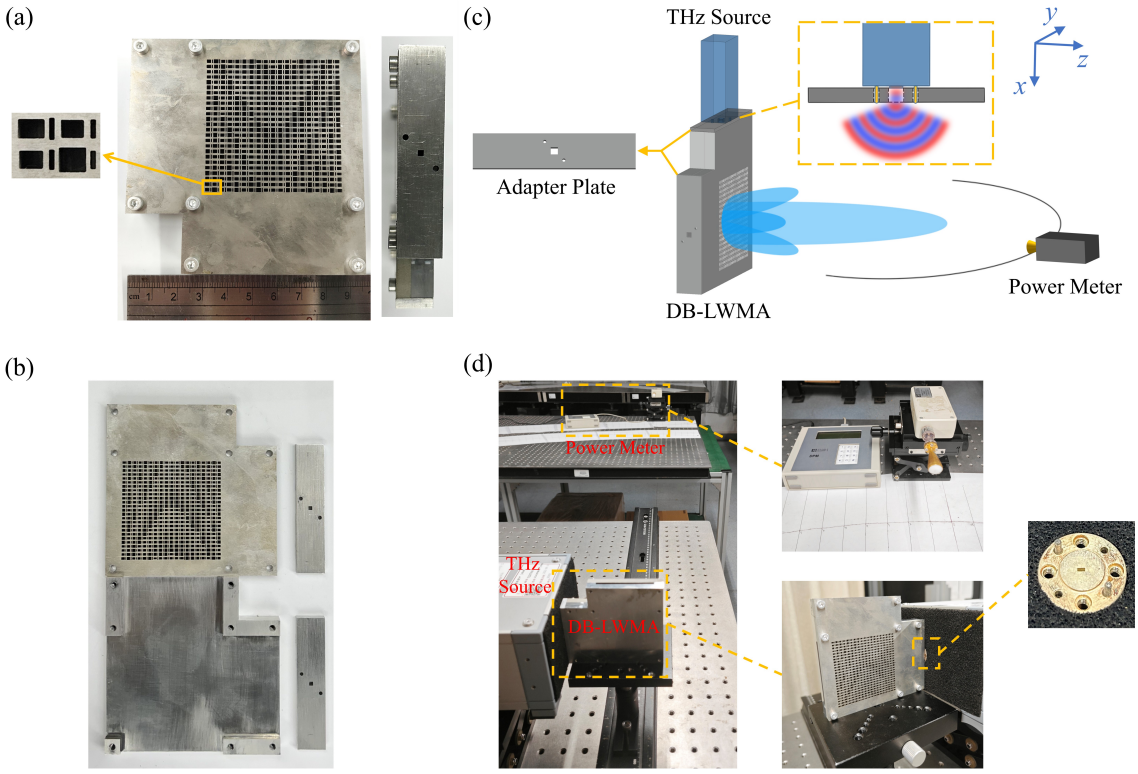

Fig. 8. (a) Fabricated prototype of DB-LWMA. (b) Top view of its two separated components and two adapter plates. Far-field radiation gain measurement setup for the THz emission antenna: (c) Schematic illustration and (d) physical photograph of the experimental setup including the DB-LWMA, THz source, and power meter, illustrating actual arrangement during the far-field measurement.

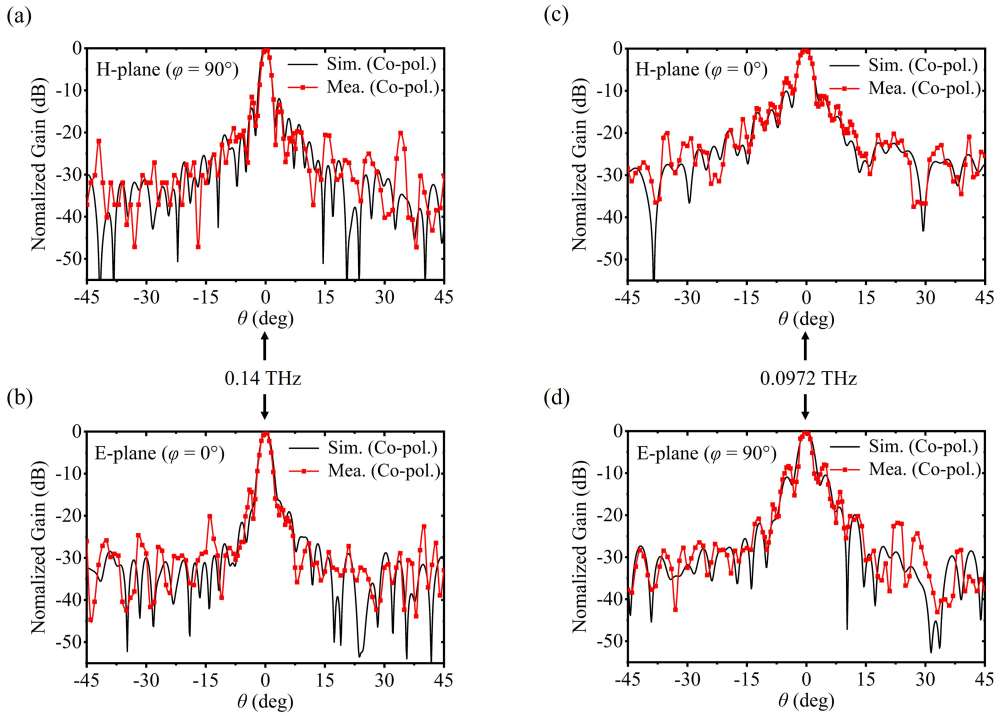

Fig. 9. Normalized radiation patterns at 0.14 THz in (a) H- and (b) E-planes. Normalized radiation patterns at 0.0972 THz in (c) H- and (d) E-planes.

TABLE III
COMPARISON OF RECENT THZ LWAS

Reference	Frequency (THz)	Dimension ($\lambda \times \lambda$)	Max. Gain (dBi)	Band (amount)
[28]	0.15–0.3	15 × 15	24.3	Single
[29]	0.43–0.56	15.6 × 0.8	16.8	Single
[30]	0.26–0.33	5.56 × 0.36	18	Single
[31]	0.132–0.146	21 × 21	33.3	Single
[46]	0.22–0.3	27.6 × 27.6	28.5	Single
our work	0.13–0.146 & 0.096–0.1	24.3 × 24.3 & 16.8 × 16.8	35.1 & 32	Dual

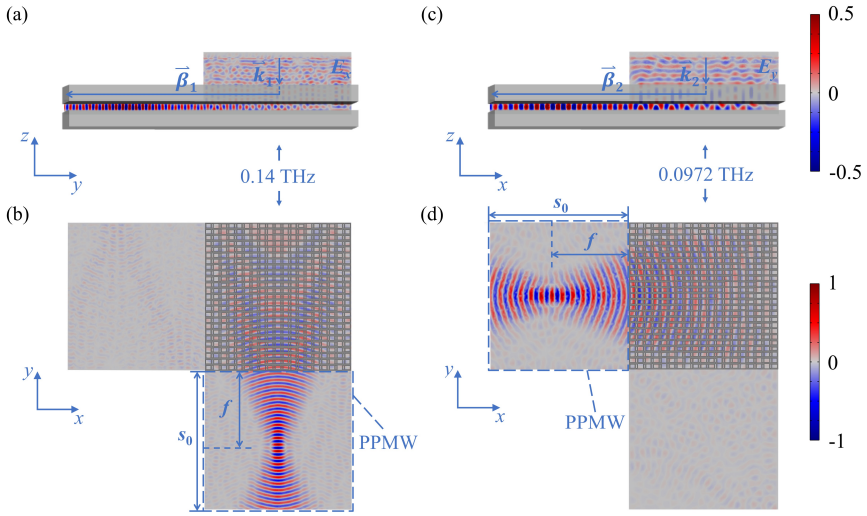

Fig. 10. DB-LWMA operating in reception mode. Electric field distributions of x-polarized waves at frequency of 0.14 THz in (a) y-z and (b) x-y planes. Electric field distributions of y-polarized waves at frequency of 0.0972 THz in (c) x-z and (d) x-y planes.

plates are shown in Fig. 8(b). The far-field measurement setup is illustrated schematically in Fig. 8(c) and the physical photograph is shown in Fig. 8(d). In the measurement, an adapter plate with an aperture of 3 mm × 3 mm was used to connect an impact-ionization avalanche transit-time (IMPATT) diode operating at the frequency of 0.14 THz and the DB-LWMA.The adapter plate can couple x-polarized waves coming from the IMPATT diode into the DB-LWMA directly through one input port. A THz power meter was employed for point-by-point measurements of the radiation intensities in the far field (3.3 m away from the antenna), which were shifted along an arc at angle intervals of 0.5° near the main lobe and 1° elsewhere. Normalized radiation patterns in H- and E-planes were obtained based on the measured results, as shown in Figs. 9(a) and 9(b), respectively. The simulated radiation patterns are also presented for comparison, and they are in good agreement. The deviations emerging at large elevation angles primarily arise from the processing errors. Similarly, y-polarized waves coming from the IMPATT diode working at the frequency of 0.0972 THz can be coupled into the DB-LWMA through the other input port. The far-field intensities were measured in the same way, and the radiation patterns in H- and E-planes were presented in Figs. 9(c) and 9(d). The simulated and measured results also agree well with each other. Compared with recent THz leaky-wave antennas summarized in Table III, the DB-LWMA first achieves co-aperture control of dual-band THz waves.

B. Reception

According to the principle of electromagnetic reciprocity, the DB-LWMA can also be used to convert free-space waves into 2D guided waves, thereby functioning as a THz receiving antenna. When x-polarized waves at the frequency of 0.14 THz are normally incident on the meta-slot array, as shown in Fig. 10(a), they can be converted into a 2D guided mode in one PPMW. At the same time, their phase can be manipulated by the meta-slots to compensate for the phase differences of the guided wave propagating from different meta-slots to the target focal point, which can be calculated based on Eq. 2. As a result, the 2D guided mode can focus within the PPMW, as shown in Fig. 10(b). Because the meta-slots can manipulate the phases of two orthogonally polarized waves independently, incident y-polarized waves at the frequency of 0.0972 THz can also be focused in the other PPMW, as shown in Figs. 10(c) and 10(d). In simulations, to better observe in-waveguide beam focusing, the lengths s_0 of the PPMWs

This article has been accepted for publication in Journal of Lightwave Technology. This is the author's version which has not been fully edited and content may change prior to final publication. Citation information: DOI 10.1109/JLT.2025.3620946

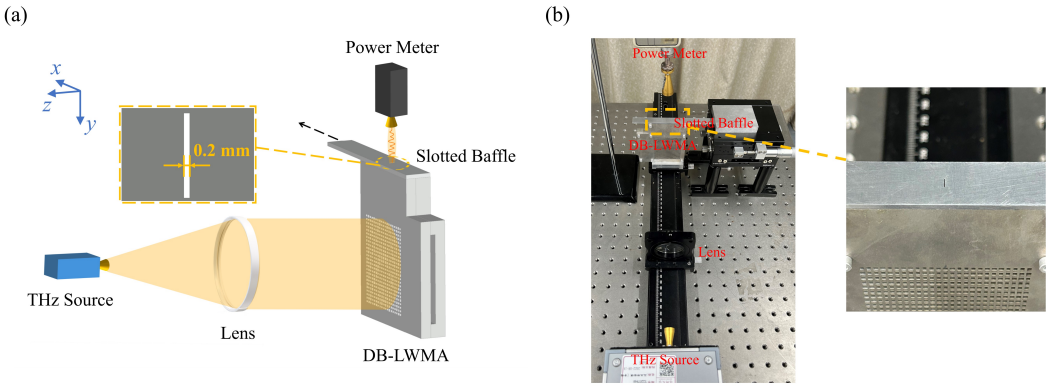

Fig. 11. (a) Schematic diagram and (b) physical photograph of the experimental setup including the DB-LWMA, THz source, slotted baffle, lens, and power meter, illustrating actual arrangement during the focusing measurement.

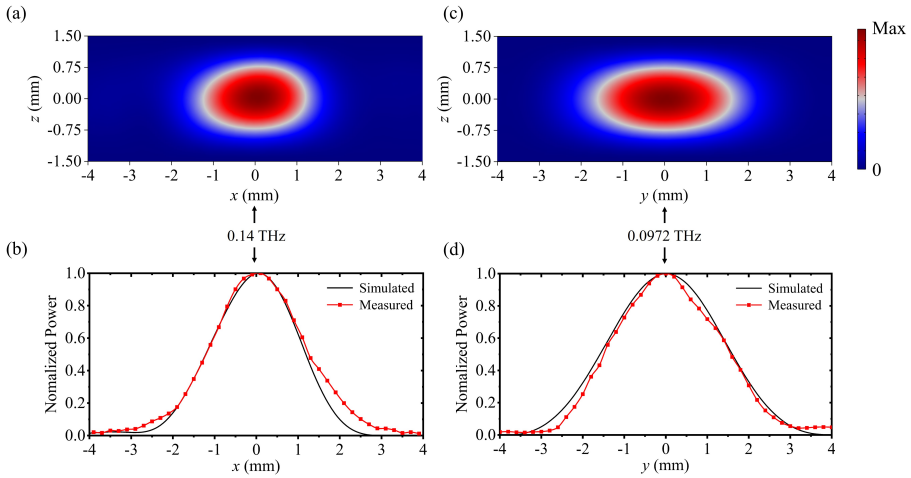

Fig. 12. DB-LWMA for focusing received THz waves into the PPMW. (a) Simulated energy distribution of the 0.14 THz beam on the focal plane. (b) Measured vs simulated power distribution curves for the 0.14 THz focal spot. (c) Simulated energy distribution of the 0.0972 THz beam on the focal plane. (d) Measured vs simulated power distribution curves for the 0.0972 THz focal spot.

were both set to 50 mm, which were greater than the focal lengths, f. However, to facilitate the measurement on the focal planes, the lengths of the PPMWs in the fabricated DB-LWMA prototype are equal to the focal lengths. The field-intensity distributions on the focal planes are displayed in Figs. 12(a) and 12(c). Compared with the incident waves, the gains at the focal points are 27 dB and 26.3 dB at the frequencies of 0.14 THz and 0.0972 THz, respectively, and the corresponding conversion efficiencies (ratio of the power on focal planes to the input power) are 48.9% and 50.8%. These efficiencies are comparable to those of commercial high-density polyethylene lenses for free-space focusing. Unlike conventional lenses for focusing in free space, the DB-LWMA achieves in-waveguide focusing in the PPMW.

To verify the design above, an experimental setup was further developed to measure the field distributions on the focal planes. The corresponding schematic diagram and physical photograph of the experimental setup are displayed in Figs. 11(a) and 11(b). In the focusing measurement of x-polarized waves, a commercial lens was used to collimate radiation waves from the IMPATT diode operating at the frequency of 0.14 THz, which was then normally incident on the meta-slot array. The waves in free space were converted into 2D guided waves and further focused on one output port of the DB-LWMA due to the phase control of the meta-slots. A baffle with a slit of 0.2 mm × 3 mm was positioned at the corresponding output port and shifted point-by-point along the x-axis with displacement accuracy of 0.2 mm. A THz power meter was used to measure the radiation power from the slit, which was placed about 7 cm from the slit. The measured and simulated field distributions are both shown in Fig. 12(b), and the full widths at half maximum (FWHMs) in the x-axis direction are 2.5 mm and 2.4 mm, respectively. To measure the field distribution of y-polarized waves, another IMPATT diode operating at the frequency of 0.0972 THz was employed. The incident waves were focused on the other output port of the DB-LWMA. The adopted measuring method is similar to that for measuring the x-polarized waves. The measured and simulated field distributions are shown in Fig. 12(d), and the FWHMs in the y-axis direction are 3.1 mm and 3.2 mm,

respectively. The measured and simulated results agree well with each other, and the minor deviation primarily originates from the processing error.

IV. Conclusion

In summary, a DB-LWMA has been presented to achieve high-gain co-aperture control of dual-band THz waves. The antenna can realize bidirectional conversion between guided and free-space waves, and can also control dual-band THz waves simultaneously and independently by arranging the meta-slots. When it operates in the transmission mode, the far-field gains and AEs are 35.1 dBi and 43.8% at 0.14 THz and 32 dBi and 44.6% at 0.0972 THz, respectively. The corresponding cross-polarization levels are –42.8 dB and –31.2 dB below the main lobes, and the isolation levels are as low as –31.3 dB and –31.1 dB. In the reception mode, the device demonstrates focal gains of 27 dB at 0.14 THz and 26.3 dB at 0.0972 THz, with conversion efficiencies of 48.9% and 50.8%, respectively. The measured and simulated results in the transmission and reception modes both agree well with each other. This innovative DB-LWMA provides new insights and solutions to address spectral scarcity and transmission distance limitations in the future ultra-high-speed THz wireless communications.

Appendix

The following abbreviations are used in this manuscript:

LWMA	Leaky-Wave Meta-Antenna
THz	Terahertz
1D	One-Dimensional
2D	Two-Dimensional
DB-LWMA	Dual-Band Leaky-Wave Meta-Antenna
PPMW	Parallel-Plate Metal Waveguide
AE	Aperture Efficiency
TE	Transverse Electric
WEDM	Wire Electrical Discharge Machining
IMPATT	Impact-Ionization Avalanche Transit-Time
FWHM	Full Width at Half Maximum

References

[1] E. Ruzomberka, D. J. Love, C. G. Brinton, A. Gupta, C.-C. Wang, and H. V. Poor, "Challenges and opportunities for beyond-5G wireless security," *IEEE Security & Privacy*, vol. 21, no. 5, pp. 55–66, 2023.

[2] T. Nagatsuma, G. Ducournau, and C. C. Renaud, "Advances in terahertz communications accelerated by photonics," *Nature Photonics*, vol. 10, no. 6, pp. 371–379, 2016.

[3] T. Kürner and S. Priebe, "Towards THz communications-status in research, standardization and regulation," *Journal of Infrared, Millimeter, and Terahertz Waves*, vol. 35, no. 1, pp. 53–62, 2014.

[4] X. Cai, X. Cheng, and F. Tufvesson, "Toward 6G with terahertz communications: Understanding the propagation channels," *IEEE Communications Magazine*, vol. 62, no. 2, pp. 32–38, 2024.

[5] M. Zhu, J. Zhang, B. Hua, M. Lei, Y. Cai, L. Tian, D. Wang, W. Xu, C. Zhang, Y. Huang *et al.*, "Ultra-wideband fiber-THz-fiber seamless integration communication system toward 6G: architecture, key techniques, and testbed implementation," *Science China Information Sciences*, vol. 66, no. 1, art. 113301, 2023.

[6] J. Lyu, S. Shen, L. Chen, Y. Zhu, and S. Zhuang, "Frequency selective fingerprint sensor: the Terahertz unity platform for broadband chiral enantiomers multiplexed signals and narrowband molecular AIT enhancement," *PhotoniX*, vol. 4, no. 1, art. 28, 2023.

[7] J. Liang, T. Ning, J. Fan, Z. Wu, M. Zhang, H. Su, Y.-J. Zeng, and H. Liang, "Metallic waveguide transmitarray antennas for generating multibeams with high gain and optional polarized states in the F-band," *Journal of Lightwave Technology*, vol. 39, no. 22, pp. 7210–7216, 2021.

[8] X. Fu, F. Yang, C. Liu, X. Wu, and T. J. Cui, "Terahertz beam steering technologies: from phased arrays to field-programmable metasurfaces," *Advanced Optical Materials*, vol. 8, no. 3, art. 1900628, 2020.

[9] J. F. Federici, B. Schulkin, F. Huang, D. Gary, R. Barat, F. Oliveira, and D. Zimdars, "THz imaging and sensing for security applications—explosives, weapons and drugs," *Semiconductor Science and Technology*, vol. 20, no. 7, pp. S266–S280, 2005.

[10] G. K. Varotsos, K. Aidinis, and H. E. Nistazakis, "Average BER performance estimation of relayed THz links with losses, molecular attenuation, adverse weather conditions, turbulence and generalized pointing errors," *Photonics*, vol. 9, no. 10, art. 671, 2022.

[11] J. Yu, Y. Wang, J. Ding, J. Zhang, W. Li, F. Wang, C. Wang, K. Wang, Y. Tan, M. Zhu *et al.*, "Broadband photon-assisted terahertz communication and sensing," *Journal of Lightwave Technology*, vol. 41, no. 11, pp. 3332–3349, 2023.

[12] D. R. Jackson, C. Caloz, and T. Itoh, "Leaky-wave antennas," *Proceedings of the IEEE*, vol. 100, no. 7, pp. 2194–2206, 2012.

[13] S. Sengupta, D. R. Jackson, A. T. Almutawa, H. Kazemi, F. Capolino, and S. A. Long, "Radiation properties of a 2-d periodic leaky-wave antenna," *IEEE Transactions on Antennas and Propagation*, vol. 67, no. 6, pp. 3560–3573, 2019.

[14] S. Tofani and W. Fuscaldo, "Fabry-perot cavity leaky wave antennas with tunable features for terahertz applications," *Condensed Matter*, vol. 5, no. 1, art. 11, 2020.

[15] G. P. Carrara, C. L. Zekios, and S. V. Georgakopoulos, "A TM 11 high-order mode leaky wave antenna," *IEEE Transactions on Antennas and Propagation*, vol. 71, no. 1, pp. 119–130, 2022.

[16] M. K. Emara and S. Gupta, "Integrated multiport leaky-wave antenna multiplexer/demultiplexer system for millimeter-wave communication," *IEEE Transactions on Antennas and Propagation*, vol. 69, no. 9, pp. 5244–5256, 2021.

[17] K. Murata, K. Murano, I. Watanabe, A. Kasamatsu, T. Tanaka, and Y. Monnai, "See-through detection and 3d reconstruction using terahertz leaky-wave radar based on

sparse signal processing," *Journal of Infrared, Millimeter, and Terahertz Waves*, vol. 39, no. 2, pp. 210–221, 2018.

[18] Q. Song, Z. Shen, and J. Lu, "Log-periodic monopole array with uniform spacing and uniform height," *IEEE Transactions on Antennas and propagation*, vol. 66, no. 9, pp. 4687–4694, 2018.

[19] C. Yi, Z. Wang, Y. Shi, S. Wan, J. Tang, W. Hu, Z. Li, Y. Zeng, Q. Song, and Z. Li, "Creating topological exceptional point by on-chip all-dielectric metasurface," *Light: Science & Applications*, vol. 14, no. 1, art. 262, 2025.

[20] E. Negri, W. Fuscaldo, P. Burghignoli, and A. Galli, "An overview of design techniques for two-dimensional leaky-wave antennas," *Applied Sciences*, vol. 15, no. 4, art. 1854, 2025.

[21] Q. Zhao, C. Guclu, Y. Huang, F. Capolino, and O. Boyraz, "Experimental demonstration of directive Si3N4 optical leaky wave antennas with semiconductor perturbations," *Journal of Lightwave Technology*, vol. 34, no. 21, pp. 4864–4871, 2016.

[22] H. Hashiguchi, T. Baba, and H. Arai, "Optical beam expander with parabolic photonic bandgap reflector for efficient excitation of optical leaky wave antenna," *Journal of Lightwave Technology*, vol. 37, no. 9, pp. 2094–2099, 2019.

[23] H. Hashiguchi, K. Kondo, T. Baba, and H. Arai, "An optical leaky wave antenna by a waffled structure," *Journal of Lightwave Technology*, vol. 35, no. 11, pp. 2273–2279, 2017.

[24] A. A. Oliner, "Leakage from higher modes on microstrip line with application to antennas," *Radio Science*, vol. 22, no. 6, pp. 907–912, 1987.

[25] I. Shahzadi, D. Comite, M. V. Kuznetcov, and S. K. Podilchak, "Compact dual-polarized fabry–perot leaky-wave antenna for full-duplex broadband applications," *IEEE Antennas and Wireless Propagation Letters*, vol. 23, no. 9, pp. 2693–2697, 2024.

[26] T. Zhao, D. R. Jackson, and J. T. Williams, "2-d periodic leaky-wave antennas-part ii: Slot design," *IEEE Transactions on Antennas and Propagation*, vol. 53, no. 11, pp. 3515–3524, 2005.

[27] N. J. Karl, R. W. McKinney, Y. Monnai, R. Mendis, and D. M. Mittleman, "Frequency-division multiplexing in the terahertz range using a leaky-wave antenna," *Nature Photonics*, vol. 9, no. 11, pp. 717–720, 2015.

[28] H. Guerboukha, R. Shrestha, J. Neronha, O. Ryan, M. Hornbuckle, Z. Fang, and D. Mittleman, "Efficient leaky-wave antennas at terahertz frequencies generating highly directional beams," *Applied Physics Letters*, vol. 117, no. 26, art. 261103, 2020.

[29] W. Hongjian, Y. Min, and M. Minzheng, "Terahertz groove gap waveguide leaky wave antenna," *Microwave and Optical Technology Letters*, vol. 65, no. 1, pp. 213–216, 2023.

[30] P. Lu, T. Haddad, B. Sievert, B. Khani, S. Makhlouf, S. Dülme, J. F. Estévez, A. Rennings, D. Erni, U. Pfeiffer *et al.*, "Inp-based thz beam steering leaky-wave antenna," *IEEE Transactions on Terahertz Science and Technology*, vol. 11, no. 2, pp. 218–230, 2020.

[31] T. Peng, L. Zhang, N. Wang, W. Chen, M. Zhang, H. Su, L. Li, and H. Liang, "Terahertz metallic waveguide with meta-holes for bidirectional conversion between two-dimensional guided waves and free-space waves," *Applied Physics Letters*, vol. 124, no. 12, art. 121702, 2024.

[32] W. Chen, Z. Feng, M. Fan, and Y. Furuya, "Dual-band reconfigurable antenna for wireless communications," *Microwave and Optical Technology Letters*, vol. 40, no. 6, pp. 503–505, 2004.

[33] X. Quan, R. Li, Y. Cui, and M. M. Tentzeris, "Analysis and design of a compact dual-band directional antenna," *IEEE Antennas and Wireless Propagation Letters*, vol. 11, pp. 547–550, 2012.

[34] M. Ding, R. Jin, J. Geng, X. Guo, and J. Chen, "A high-gain dual-band directional/omnidirectional reconfigurable antenna for wlan systems," *International Journal of RF and Microwave Computer-aided Engineering*, vol. 18, no. 3, pp. 225–232, 2008.

[35] Y. Ding and K. W. Leung, "On the dual-band dra-slot hybrid antenna," *IEEE Transactions on Antennas and Propagation*, vol. 57, no. 3, pp. 624–630, 2009.

[36] Z. Xiao, Q. Yang, J. Huang, Z. Huang, W. Zhou, Y. Gao, R. Shu, and Z. He, "Terahertz communication windows and their point-to-point transmission verification: publisher's note," *Applied Optics*, vol. 57, no. 29, pp. 8593–8593, 2018.

[37] S. Aliaga, V. Petrov, and J. M. Jornet, "Cross-link interference modeling in 6g millimeter wave and terahertz leo satellite communications," in *Proc. IEEE International Conference on Communications (ICC)*, pp. 2577–2582, 2023.

[38] G. Xu, A. Overvig, Y. Kasahara, E. Martini, S. Maci, and A. Alù, "Arbitrary aperture synthesis with nonlocal leaky-wave metasurface antennas," *Nature Communications*, vol. 14, no. 1, art. 4380, 2023.

[39] F. Monticone and A. Alu, "Leaky-wave theory, techniques, and applications: From microwaves to visible frequencies," *Proceedings of the IEEE*, vol. 103, no. 5, pp. 793–821, 2015.

[40] M. A. Ordal, R. J. Bell, R. W. Alexander Jr, L. A. Newquist, and M. R. Querry, "Optical properties of Al, Fe, Ti, Ta, W, and Mo at submillimeter wavelengths," *Applied Optics*, vol. 27, no. 6, pp. 1203–1209, 1988.

[41] J. Liang, T. Ning, J. Fan, M. Zhang, H. Su, Y.-J. Zeng, and H. Liang, "Metallic waveguide transmitarrays for dual-band multibeam terahertz antennas," *Applied Physics Letters*, vol. 119, no. 25, art. 253501, 2021.

[42] H. Liang, J. Li, Z. Wu, L. Zhang, and S. Ruan, "Metallic waveguide arrays for metasurface-like control with high simplicity in design," *Advanced Optical Materials*, vol. 8, no. 18, art. 2000605, 2020.

[43] H. A. Malhat, A. S. Elhenawy, S. H. Zainud-Deen, and N. A. El-Shalaby, "1-D reconfigurable graphene-strips leaky-wave antenna with different feeders for wide scanning angles," *International Journal of RF and Microwave Computer-Aided Engineering*, vol. 31, no. 7, art. e22683,

2021.

[44] H. Li, J. Xiong, and S. He, "A compact planar mimo antenna system of four elements with similar radiation characteristics and isolation structure," *IEEE Antennas and Wireless Propagation Letters*, vol. 8, pp. 1107–1110, 2009.

[45] C. Qi and A. M. Wong, "Simultaneously enhancing radiation and aperture efficiencies of leaky wave antennas using discrete metasurfaces," *IEEE Transactions on Antennas and Propagation*, vol. 73, no. 9, pp. 6403–6413, 2025.

[46] A. Gomez-Torrent, M. Garcia-Vigueras, L. Le Coq, A. Mahmoud, M. Ettorre, R. Sauleau, and J. Oberhammer, "A low-profile and high-gain frequency beam steering subterahertz antenna enabled by silicon micromachining," *IEEE Transactions on Antennas and Propagation*, vol. 68, no. 2, pp. 672–682, 2019.